

Polychromatic image fusion algorithm and fusion metric for automatized microscopes

Mario A. Bueno

CITEDI-IPN
2498 Roll Drive #757
Otay Mesa
San Diego, California
and
CICESE
Dirección de Telemática
Km. 107 Carretera Tijuana-Ensenada
Ensenada, B.C. México, CP 22860

Josué Álvarez-Borrego

CICESE
Dirección de Telemática
Km. 107 Carretera Tijuana-Ensenada
Ensenada, B.C. México, CP 22860
E-mail: josue@cicese.mx

Leonardo Acho

CITEDI-IPN
2498 Roll Drive #757
Otay Mesa
San Diego, California

María Cristina Chávez-Sánchez

Unidad Mazatlán en Acuicultura y Manejo
Ambiental
Centro de Investigación en Alimentación y
Desarrollo, A. C.
Sábalo Cerritos S/N
Apdo. Postal 711, Estero del Yugo
Mazatlán Sinaloa, C.P. 82010, México

1 Introduction

Automated systems are required when researchers in medical and biological areas analyze a great number of micro-biological samples; therefore, automated devices that can systematically analyze large numbers of these samples would be beneficial and lessen the amount of time for analysis.

The primary optical tool used to analyze a wide variety of microscopic samples is the light microscope. An automated microscope can automatically capture and process images of a sample, where one of the goals of this process is to obtain the best sample image with which to work. However, due to the high number of biological samples available and their volumetric structures, more than one image captured in the Z axis direction contains relevant and useful information. With these multiple images, we can construct a high-quality image instead of relying on and using the best focused image. In this context, the image

Abstract. We propose a new algorithm to determine the multifocus image fusion from several polychromatic images captured from the best focusing region where the best in focus image is included from a biological sample. This focusing region is built by including several images up and down starting from the Z position of the best image in focus. These captured RGB images are converted to $YCbCr$ color space to have the color $CbCr$ and intensity Y channels separated with the objective to preserve the color information of the best in focus image. Several approaches have been developed to fuse images, like those algorithms based on the wavelets transform, Laplacian, ratio, contrast or morphological pyramids selection, fusion by averaging, Bayesian methods, fuzzy sets, and artificial networks. However, this algorithm utilizes the Fourier approach by using the Y channel frequency content via analyzing the Fourier coefficients to retrieve the high frequencies to obtain the best possible characteristics of every captured image. After the completion of this process, we continue to construct the fused image with these coefficients and color information for the optimum in focus image in the $YCbCr$ color space; as a result, we obtain a precise final RGB fused image. © 2005 Society of Photo-Optical Instrumentation Engineers. [DOI: 10.1117/1.2048708]

Subject terms: automatized microscope; fusion algorithms; multifocus image fusion; $YCbCr$ color space; Fourier transform; fusion metrics; fusion quality measures.

Paper 040618RR received Sep. 1, 2004; revised manuscript received Mar. 3, 2005; accepted for publication Mar. 10, 2005; published online Sep. 16, 2005.

fusion concept emerges. The image fusion process is similar to the combination of two or more images into a single image where one retains the relevant information from each captured image.¹

Some important applications of image fusion are related with military, surveillance, computer vision, robotics, medical imaging, remote sensing, and microscopic imaging fields. Studies have found several fusion methods previously developed.¹⁻¹⁰ These methods use different approaches to obtain the image fusion, some of them are based on the wavelets transform, Laplacian, ratio, contrast or morphological pyramids selection, fusion by averaging, Bayesian methods, fuzzy sets, and artificial networks.¹⁻¹⁰ However, the image fusion algorithm proposed in this paper is based on the Fourier transform approach. To measure the final fused image quality, a fusion metric is described based on developed index proposed by Wang and Bovik¹¹ and Piella and Heijmans.¹²

Section 2 provides the mathematical support for the proposed images fusion algorithm as well as the color space used to fuse polychromatic images. Section 3 describes

some metrics used to measure the final image-fused quality generated by the proposed image fusion algorithm. Section 4 describes the computational experiments and provides the results of those experiments where we illustrate the enhancement of the fused image of proposed algorithm tested by the authors. Finally, Sec. 5 summarizes our conclusion and future work.

2 New Multifocus Fusion Algorithm Based on Fourier Transform

Let us introduce some useful notation, definitions, and functions: S_W is a stack of W polychromatic captured images of size $N \times M$ pixels from a biological sample taken by stepping in the microscope in the Z axis direction at Δz increments; $f_1, f_2, f_3, \dots, f_K$ is a subset from S_W with K images to fuse, this subset is called the best in focus region (BFR). The BFR contains the best in focus captured images and best in focus image f_{BF} obtained with an autofocus algorithm.¹³⁻²⁰ The BFR can be constructed selecting ξ quantity of images, where ξ will be the captured images selected up and down from f_{BF} in the Z axis direction. Therefore, $K=2\xi+1$ images to fuse, where $K < W$ and f_{BF} are positioned inside $f_1, f_2, f_3, \dots, f_K$ with $f_{\lfloor K/2 \rfloor + 1} = f_{BF}$, where $\lfloor \tau \rfloor$ is an integer function of a number τ ; $f^{RGB}(x, y)_k$ is the k th captured image matrix with pixels (x, y) inside the BFR, thus $f^{RGB}(x, y)_k \in \text{BFR} \subset S_W$, where $x=1, 2, \dots, N$, $y=1, 2, \dots, M$, and $k=1, 2, \dots, K$. Finally, $f^R(x, y)_k, f^G(x, y)_k, f^B(x, y)_k$ are the RGB decomposition channels, respectively, of $f^{RGB}(x, y)_k$ with range $[0, 255]$, where red R , green G , and blue B are channels in the RGB color space representation.

2.1 Color Space Representation Suitable to Solve a Fusion Problem

In 1931 the Commission Internationale de l'Eclairage (CIE) developed a standard primary color reference with three R, G , and B monochromatic channels,²¹ however, in this paper, we use the NTSC 24-bit RGB CRT color space standard, where every 8-bit channel values has a range 0 to 255. This RGB color space image representation is used by some digital devices such as cameras to integrate a color digital image saved in a tridimensional matrix $f^{RGB}(x, y)$. The color information is fully correlated by RGB channels; however, the RGB color space representation is not suitable to solve some problems, when color and intensity information should be separated. Several applications were developed using different color space representations. As a recent example, one can notice that Nikulin and Bebis developed an image retrieval application, where the application was based on usage of the RGB and YIQ color spaces manipulation via the wavelet transform.²²

In this paper, we propose to use the $YCbCr$ color space representation, and not the YIQ color space or another color space to obtain the final fused image from the BFR, because it has a 16 to 235 nominal range when performing $YCbCr$ -to- RGB conversion, this prevents going outside the 0 to 255 range, due to video processing problem and noise generated by electronic changes, so $YCbCr$ color space is used in this context to avoid underflow and overflow wrap-around problems.^{23,24}

Let us define $\mathbf{f}^{YCbCr}(x, y)$ to be an image in the $YCbCr$ color space representation and $f^Y(x, y), f^{Cb}(x, y)$, and $f^{Cr}(x, y)$ their respective integrating channels. However, there are several $YCbCr$ sampling formats, such as 4:4:4, 4:2:2, 4:1:1, and 4:2:0. The matrix conversion used in this paper is an alternative to represent RGB to $YCbCr$ for SDTV (Standard definition TV, 4:2:2 sampling format) under the new CCIR-601 encoder format.^{23,24} This RGB to $YCbCr$ and vice versa matrix conversion have new uses on this type of image processing algorithms, as described in the paper of Kober et al.²⁵ The RGB -to- $YCbCr$ and $YCbCr$ -to- RGB color space conversions,²¹ can be expressed by

$$\mathbf{f}^{YCbCr}(x, y) = \begin{bmatrix} 0.299 & 0.587 & 0.144 \\ -0.169 & -0.331 & 0.5 \\ 0.5 & -0.419 & -0.081 \end{bmatrix} \begin{bmatrix} f^R(x, y) \\ f^G(x, y) \\ f^B(x, y) \end{bmatrix}, \quad (1)$$

and

$$\mathbf{f}^{RGB}(x, y) = \begin{bmatrix} 1 & -0.0009 & 1.4 \\ 1 & -0.344 & -0.714 \\ 1 & 1.772 & 0.001 \end{bmatrix} \begin{bmatrix} f^Y(x, y) \\ f^{Cb}(x, y) \\ f^{Cr}(x, y) \end{bmatrix}, \quad (2)$$

where $\mathbf{f}^{YCbCr}(x, y)$ is the $YCbCr$ color space representation of $\mathbf{f}^{RGB}(x, y)$ and $\mathbf{f}^{RGB}(x, y)$ is the RGB color space representation of $\mathbf{f}^{YCbCr}(x, y)$, when $x=1, 2, \dots, N$ and $y=1, 2, \dots, M$. Thus, $f^Y(x, y)$ is the intensity or luminance channel with working range $[0, 255]$, while $f^{Cb}(x, y)$ and $f^{Cr}(x, y)$ are the color or chrominance channels with working range $[-128, 127]$. Let us define some useful notation to represent the color space conversions defined in Eqs. (1) and (2). In this sense, $\Phi^{YCbCr}\{\mathbf{f}^{RGB}(x, y)\}$ is defined to be the conversion $RGB \rightarrow YCbCr$ image function expressed in notational form by

$$\mathbf{f}^{YCbCr}(x, y) = \Phi^{YCbCr}\{\mathbf{f}^{RGB}(x, y)\}, \quad (3)$$

while $\Phi^{RGB}\{\mathbf{f}^{YCbCr}(x, y)\}$ is defined to be the conversion $YCbCr \rightarrow RGB$ image function written in notational form by

$$\mathbf{f}^{RGB}(x, y) = \Phi^{RGB}\{\mathbf{f}^{YCbCr}(x, y)\}. \quad (4)$$

2.2 New Multifocus Fusion Algorithm

We propose an algorithm to fuse polychromatic images based on the spectral analysis of RGB images transformed to $YCbCr$ color space representation, where color and intensity information are perfectly separated. Currently, several fusion techniques are based in alternative techniques, i.e., wavelets, ratio, average, pyramids, etc. The Fourier transform is a robust tool, well proved over several decades and never has been used, to our knowledge, for image fusion algorithm development. However, we decided to test a hypothesis where it is possible to have a high-performance algorithm based on spectral analysis via fast Fourier transform (FFT), capable to achieve improved results from multiple images to be fused, like those results given in Table 1 compared with the results obtained from other techniques, which are shown in the same table.²⁶ The FFT gives us a

Table 1 Fusion quality measures Q , Q_{Wt} , and Q_E results that were obtained by the Laplacian gradient, the ratio pyramid, the discrete wavelet transform (DWT), the average pyramid fusion techniques, the discrete cosine transform (DCT), and the proposed fusion algorithm.

Measures	Laplacian	Ratio	DWT	Average	DCT	Proposed fusion algorithm
Q	0.9010	0.7900	0.8920	0.8640	0.9465	0.9739
Q_{Wt}	0.9290	0.8300	0.9240	0.9010	0.9464	0.9738
Q_E	0.8450	0.6680	0.8390	0.7450	0.8545	0.9292

more highly sensible analysis of frequency coefficients from the images involved in the fusion algorithm than the DCT, and with the FFT, the final fused image is constructed with higher definition. Thus, the main proposed contribution in this paper is a new high-performance fusion algorithm based on spectral analysis via FFT that is easy to implement.

Let us obtain $\mathbf{f}_{BF}^{YCbCr}(x,y) = \Phi^{YCbCr}\{f_{BF}\}$, where $f_{BF}^{YCbCr}(x,y)$ is the best image in focus transformed in $YCbCr$ color space representation and their respective $f_{BF}^Y(x,y)$, $f_{BF}^{Cb}(x,y)$, and $f_{BF}^{Cr}(x,y)$ $YCbCr$ integrated channels. After obtaining $\mathbf{f}_{BF}^{YCbCr}(x,y)$, we continue getting the $YCbCr$ color space representations of $f_1, f_2, f_3, \dots, f_K$ images by the expression

$$\mathbf{f}^{YCbCr}(x,y)_k = \Phi^{YCbCr}\{f(x,y)_k\} \text{ for } k = 1, 2, \dots, K. \quad (5)$$

Once we have $f_1, f_2, f_3, \dots, f_K$ images transformed to $YCbCr$ color space representation according Eq. (5), we obtain their respective $f^Y(x,y)_k, f^{Cb}(x,y)_k$, and $f^{Cr}(x,y)_k$ $YCbCr$ integrated channels.

The final fused image $\mathbf{f}^{RGB^*}(x,y)$ can be obtained by

$$\mathbf{f}^{RGB^*}(x,y) = \Phi^{RGB}\{\mathbf{f}^{YCbCr^*}(x,y)\}, \quad (6)$$

where $\mathbf{f}^{YCbCr^*}(x,y)$ is the fused image in $YCbCr$ color space representation, thus $\mathbf{f}^{YCbCr^*}(x,y)$ can be obtained by

$$\mathbf{f}^{YCbCr^*}(x,y) = \{f^Y(x,y) \cup f_{BF}^{Cb}(x,y) \cup f_{BF}^{Cr}(x,y)\}, \quad (7)$$

thus $\mathbf{f}^{YCbCr^*}(x,y)$ is the result of constructing a tridimensional matrix by the union of the $f^Y(x,y), f_{BF}^{Cb}(x,y)$, and $f_{BF}^{Cr}(x,y)$ channels. In this context, $f^Y(x,y)$ is the fused Y channel obtained by the magnitude of inverse Fourier transform of the fused Y channel Fourier transform $f^{Y^{**}}(u,v)$, then $f^Y(x,y)$ can be acquired by

$$f^Y(x,y) = |\mathbf{F}^{-1}\{f^{Y^{**}}(u,v)\}|. \quad (8)$$

Let $f^{Y^{***}}(u,v)_k = \mathbf{F}\{f^Y(x,y)_k\}$ be the Fourier transform of Y channel of the k 'th image inside the BFR. Therefore, $f^{Y^{**}}(u,v)$ can be obtained by the following expression

$$f^{Y^{**}}(u,v) = \begin{cases} f^{Y^{***}}(u,v)_k & \text{if } |f^{Y^{***}}(u,v)_k| \geq |f^{Y^{***}}(u,v)_{k+1}| \\ f^{Y^{***}}(u,v)_{k+1} & \text{otherwise,} \end{cases} \quad (9)$$

for $u=1, 2, \dots, N, v=1, 2, \dots, M, k=1, 2, \dots, K-1$, and $|f^{Y^{***}}(u,v)_k|$ is the Fourier magnitude of Y channel of the k 'th image. Ultimately, Eq. (9) defines the proposed algorithm kernel where the best characteristics of every image to be fused remains in $f^{Y^{**}}(u,v)$ after the process. Finally we use the f_{BF} color information to obtain the final fused image $\mathbf{f}^{RGB^*}(x,y)$. However, this algorithm analyzes all coefficients from the images where the highest energy is concentrated in two or four coefficients, which are in the low-frequency region only. But, the remaining coefficients, which have information of the high frequencies, represent the best visual characteristics of the images. For this reason, when we obtain the maximum of the magnitude of the Fourier coefficients from the images to be fused, the low frequencies have no effect on the resulting fused image.

3 Quality Metrics to Measure the Image Fusion Algorithm Results

Image fusion is a process involved with the integration of multiple images where the result is a composite image with higher visual characteristics than images used to integrate it. Therefore, how can we measure the quality of the fused image? Several metrics were defined to measure the experimental results. One such metric is the mean square error (MSE), which is widely used to make these comparisons or metrics based on the measure of the image differences.²⁷ However, a nonreference quality metric was recently introduced to measure the fusion of two images given by Wang and Bovik¹¹ and extended by Piella and Heijmans.¹² In this paper, we propose to extend the Piella and Heijmans's metric to be used when several images are fused instead of just two images.

3.1 Wang and Bovik's Fusion Metric

The Wang and Bovik metric was instrumental in the development of an image quality index where no reference image is required to measure the quality of the fused image. In this context, they concluded that the proposed metric outperforms the MSE, due to the metric's ability of measuring

structural distortions and in contrast to the MSE, which is highly sensitive and tends to introduce energy errors.¹²

They define Q_0 as an image quality index and quantify the structural distortion between images $g(x,y)$ and $h(x,y)$. We can express Q_0 as

$$Q_0 = \left(\frac{\sigma_{gh}}{\sigma_g \sigma_h} \right) \left(\frac{2 \bar{x}_g \bar{x}_h}{\bar{x}_g^2 + \bar{x}_h^2} \right) \left(\frac{2 \sigma_g \sigma_h}{\sigma_g^2 + \sigma_h^2} \right), \quad (10)$$

where $\bar{x}_g, \bar{x}_h, \sigma_g,$ and σ_h are mean and standard deviations, respectively, of images $g(x,y)$ and $h(x,y)$. In fact, the value Q_0 is a measure between $g(x,y)$ and $h(x,y)$ similarity, where Q_0 takes values from 1 to -1 . Three components are recognized in Eq. (10): $(\sigma_{gh}/\sigma_g \sigma_h)$ is the correlation coefficient between $g(x,y)$ and $h(x,y)$ having a range to $[-1, 1]$; $(2 \bar{x}_g \bar{x}_h / (\bar{x}_g^2 + \bar{x}_h^2))$ is a kind of average luminance distortion, having a range to $[0, 1]$; and finally, $(2 \sigma_g \sigma_h / (\sigma_g^2 + \sigma_h^2))$ is contrast distortion measure having a range of $[0, 1]$.

Since image signals are generally nonstationary, it is convenient to calculate Q_0 over local regions and then combine the results obtained into one final result, in this sense, the authors propose to use a sliding window strategy, where the window slides one pixel at the time in the x, y direction across the entire image. Let w_s be the sliding window with size $w_x \times w_y$ pixels, for each w_s the local quality index Q_0 between $g(i,j)$ and $h(i,j)$ is computed by Eq. (10) over the pixels (i,j) , where $(i,j) \in w_s$, hence $Q_0[g(i,j), h(i,j) | (i,j) \in w_s]$ and in notational form $Q_0(g, h | w_s)$.

Therefore, the global quality index $Q_0(g, h)$ between $g(x,y)$ and $h(x,y)$, can be computed by averaging all local quality indices and can be obtained by

$$Q_0(g, h) = \frac{1}{|T|} \sum_{w_s \in T} Q_0(g, h | w_s), \quad (11)$$

where T is the family of all sliding windows computed and $|T|$ is the cardinality of T .

3.2 Piella and Heijmans's Fusion Metrics

The Piella and Heijmans's metrics use the image quality index Q_0 defined in Eq. (10) to define new quality measures that quantify the fused image f^* quality obtained by $g(x,y)$ and $h(x,y)$ fusion.

3.2.1 Piella and Heijmans's Q fusion metric

They define a new fusion quality measure given by

$$Q(g, h, f^*) = \frac{1}{|T|} \sum_{w_s \in T} [\lambda_g(w_s) Q_0(g, f^* | w_s) + \lambda_h(w_s) Q_0(h, f^* | w_s)], \quad (12)$$

where $\lambda(w_s)$ is a local weight with range $[0, 1]$, Q_0 is like Eq. (10), the subindices g and h are the two images analyzed, and $|T|$ is the cardinality of T . In this context, $Q(g, h, f^*)$ is mainly determined by similarity of f^* with the input image $g(x,y)$ when $\lambda_g(w_s)$ is higher than $\lambda_h(w_s)$ and with the input image $h(x,y)$ when $\lambda_h(w_s)$ is higher than $\lambda_g(w_s)$; however, the different quality measures obtained inside each window w_s have been treated equally, which is

opposite to the human vision, which is known to give a higher importance to visually salient regions in the image.¹²

3.2.2 Piella and Heijmans's Q_{wt} fusion metric

Piella and Heijmans defined a variant of the fusion quality measure Q where the higher image saliencies are weighted more than those with lower saliencies. Corresponding to those areas are the perceptually important parts of the underlying scene. Therefore, these areas become more relevant when the overall image quality is computed, thus, the overall saliency $Y^{ov}(g, h | w_s)$ inside a window w_s between $g(x,y)$ and $h(x,y)$, is defined as

$$Y^{ov}(g, h | w_s) = \max\{[Y(g | w_s), Y(h | w_s)]\}. \quad (13)$$

Therefore, the weighted fusion quality measure $Q_{wt}(g, h, f^*)$ between the images $g(x,y)$ and $h(x,y)$ can be expressed as

$$Q_{wt}(g, h, f^*) = \sum_{w_s \in T} c(w_s) [\lambda_g(w_s) Q_0(g, f^* | w_s) + \lambda_h(w_s) Q_0(h, f^* | w_s)], \quad (14)$$

where $c(w_s) = [Y^{ov}(g, h | w_s)] / [\sum_{w_s \in T} Y^{ov}(g, h | w_s)]$ is the weight factor.

3.2.3 Piella and Heijmans's Q_E fusion metric

Finally, Piella and Heijmans introduced a last modification of the fusion quality measure Q_{wt} to take into account some aspects of the human vision, where the edge information of the underlying scene is taken to obtain the fusion quality measure Q_E . In this approach, the edge information (e.g., the norm of the gradient) is used by Eq. (14) instead of gray-scale images. Let $g^e(x,y), h^e(x,y)$, and f^{e*} be the corresponding edge images of the images $g(x,y), h(x,y)$, and f^* , respectively, thus combining the $Q_{wt}(g, h, f^*)$ and $Q_{wt}(g^e, h^e, f^{e*})$ can be obtained from the fusion edge measure by the following expression

$$Q_E(g, h, f^*) = Q_{wt}(g, h, f^*)^{1-\alpha} Q_{wt}(g^e, h^e, f^{e*})^\alpha, \quad (15)$$

where α is the edge contribution parameter that expresses this contribution from edge images comparing with the original images. It takes values from 0 to 1 and selecting α close to 1 ensures the quality of the edge images. The $Q_E(g, h, f^*)$ index is called edge-dependent fusion quality index. All the previously described indices take on values from -1 to 1. The final fused image will have a higher composition quality from the original images the closer the index value is to 1.

3.3 Multiimage Fusion Metrics Proposed

The $Q(g, h, f^*), Q_{wt}(g, h, f^*),$ and $Q_E(g, h, f^*)$ fusion quality indices proposed by Piella and Heijmans just obtain the fusion measure from two images fused, in this case $g(x,y)$ and $h(x,y)$; however, our proposed algorithm can be used to fuse several images. Therefore, it is important to have a quality fusion measure to evaluate the fusion quality of the algorithm. We propose to extend the Piella and Heijmans's fusion quality indices to be useful to measure a multiimage fusion process.

Let $f_1, f_2, f_3, \dots, f_K \rightarrow f_{1, \dots, K}$ be the images to be fused; let $Q(f_{1, \dots, K}, f^*)$, $Q_{Wt}(f_{1, \dots, K}, f^*)$, and $Q_E(f_{1, \dots, K}, f^*)$ be the multiimage fusion quality indices proposed based on Piella and Heijmans's fusion quality indices.

3.3.1 Multiimage $Q(f_{1, \dots, K}, f^*)$ fusion metric

Let $Y(f_1|w_s), Y(f_2|w_s), \dots, Y(f_K|w_s)$ be some saliencies of images $f_{1, \dots, K}$ in window w_s and let $\lambda_{f_1}(w_s), \lambda_{f_2}(w_s), \dots, \lambda_{f_K}(w_s)$ be the local weights, these local weights can be computed as

$$\lambda_{f_1}(w_s) = \frac{Y(f_1|w_s)}{\sum_{p=1}^K Y(f_p|w_s)}, \lambda_{f_2}(w_s) = \frac{Y(f_2|w_s)}{\sum_{p=1}^K Y(f_p|w_s)}, \dots, \lambda_{f_K}(w_s) = \frac{Y(f_K|w_s)}{\sum_{p=1}^K Y(f_p|w_s)}, \quad (16)$$

then, the $Q(g, h, f^*)$ in this new metric can be written as

$$Q(f_{1, \dots, K}, f^*) = \frac{1}{|T|} \sum_{w_s \in T} \sum_{p=1}^K \lambda_{f_p}(w_s) Q_0(f_p, f^*|w_s). \quad (17)$$

3.3.2 Multiimage $Q_{Wt}(f_{1, \dots, K}, f^*)$ fusion metric

Let $Y^{ov}(f_{1, \dots, K}|w_s)$ be the overall saliency inside window w_s between the images $f_{1, \dots, K}$, shown in Sec. 3.2.2, hence it can be obtained by

$$Y^{ov}(f_{1, \dots, K}|w_s) = \max\{[Y(f_1|w_s), Y(f_2|w_s), \dots, Y(f_K|w_s)]\}, \quad (18)$$

thus, the new weighted fusion quality measure $Q_{Wt}(f_{1, \dots, K}, f^*)$ between the images $f_{1, \dots, K}$, can be expressed as

$$Q_{Wt}(f_{1, \dots, K}, f^*) = \sum_{w_s \in T} \sum_{p=1}^K c^*(w_s) \lambda_{f_p}(w_s) Q_0(f_p, f^*|w_s), \quad (19)$$

where $c^*(w_s) = [Y^{ov}(f_{1, \dots, K}|w_s)] / [\sum_{w_s \in T} Y^{ov}(f_{1, \dots, K}|w_s)]$ is the weight factor.

3.3.3 Multiimage $Q_E(f_{1, \dots, K}, f^*)$ fusion metric

Finally, let $f_1^e, f_2^e, f_3^e, \dots, f_K^e \rightarrow f_{1, \dots, K}^e$ be the corresponding edge images of the images $f_{1, \dots, K}$, therefore combining $Q_{Wt}(f_{1, \dots, K}, f^*)$ and $Q_{Wt}(f_{1, \dots, K}^e, f^{e*})$ we can obtain a new fusion edge quality index $Q_E(f_{1, \dots, K}, f^*)$, expressed as

$$Q_E(f_{1, \dots, K}, f^*) = Q_{Wt}(f_{1, \dots, K}, f^*)^{1-\alpha} Q_{Wt}(f_{1, \dots, K}^e, f^{e*})^\alpha, \quad (20)$$

where α is the edge contribution parameter defined in a similar fashion, as described in Sec. 3.2.3.

4 Computational Experiments

Sixty images integrating an image stack were captured from a microscope to test the fusion properties of the proposed algorithm. The images used were taken from a real sample utilizing a digital color CCD camera from LEICA

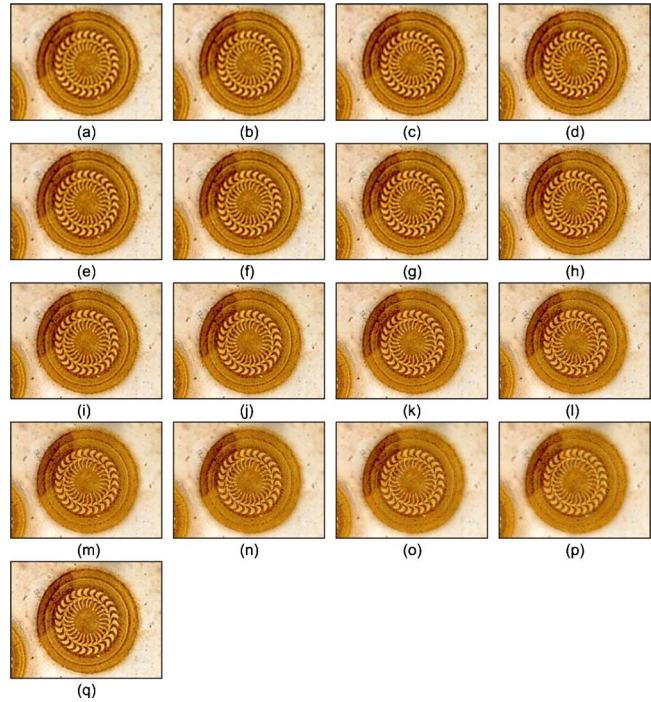


Fig. 1 (a) to (p) Images to be fused with image stack indices 23 to 38, (h) best image on focus obtained by an autofocus algorithm with image stack index 30, and (q) final fused image obtained by the proposed algorithm.

(model DC 300). The camera connected directly to a LEICA DMRXA2 microscope; on the other hand, the resolution used to take these images was 2088×1550 pixels and were captured without any previous image correctness process. The equipment used was a 2.5 GHz PC Pentium 4 with 1 GByte RAM and 80-Gbyte HD.

After the image stack was captured, it was processed by an autofocus algorithm²⁸ to obtain the best image on focus. After the focused image was obtained, we selected the images to be fused. We can say briefly that the characteristics of the new autofocus algorithm are low execution time, FFT kernel based, polychromatic and high-resolution image processing.²⁸ The selected images will shape the BFR where the fusion process will be applied. In this case, 16 images were included in the BFR from a biological microorganism from the genus *Trichodina*, a protozoan fish parasite. The proposed fusion algorithm obtained every image from the BFR and built the final fused image according to Sec. 2. Figures 1(a)–1(p) show the images that were fused by the algorithm, these images have 3-D information and are a section of a full image like that shown in Fig. 2(c). Figure 1(h) shows the best image on focus and Fig. 1(q) shows the final fused image. These images were taken with a Z increment of $0.5 \mu\text{m}$. Figure 2(c) shows the zoomed window, from the final fusion image of Fig. 2(b), compared to the best image on focus in Fig. 2(a). Figure 3 shows an additional example between the focused image of Fig. 3(a) and the fused image from a shrimp tissue sample of Fig. 3(b), where the visual differences are shown from the zoomed window in Fig. 3(c).

Thus, to measure the proposed algorithm performance, we extended the fusion quality measures, as already cited,

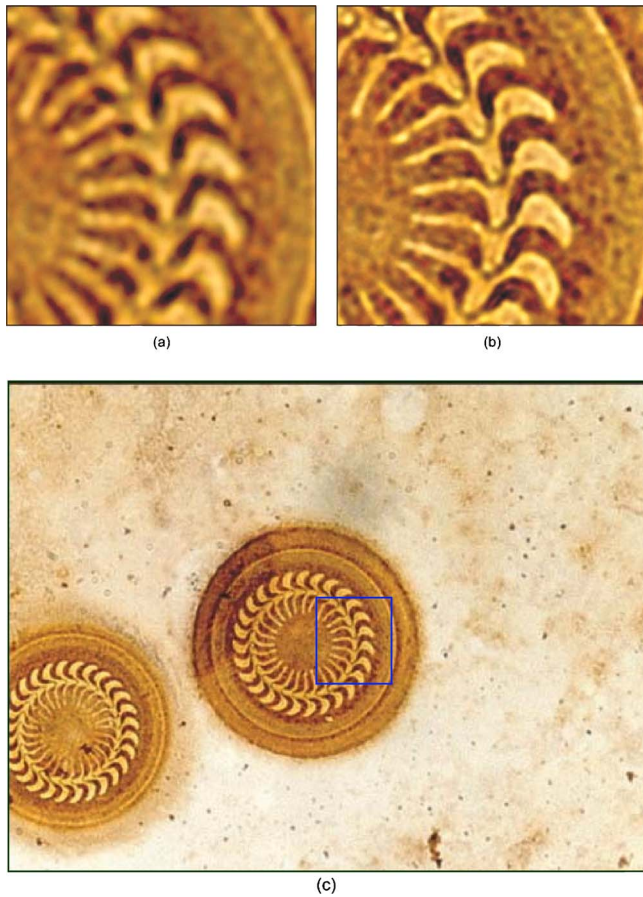


Fig. 2 Example of visual differences inside zoomed window shown in (c), between (a) the focused image and (b) the fused image from *Trichodine* sample.

to obtain new fusion quality measures capable of measuring a multiimage fusion process, as described in this paper. The result obtained was that the proposed algorithm has higher performance to fuse real images, as displayed in Table 1. Three fusion quality measures Q , Q_{Wt} , and Q_E were used to measure the fusion process. The Q index is related to the algorithm's capacity to take advantage of image characteristics in general manner due to the Q index taking all local window measures from images in equal form. In this sense the Q_{Wt} and Q_E indices are related to algorithm capacity to take advantage of image visual characteristics and edge information, respectively, and these indices take into account some aspect of human visual system.¹² Thus, the extended fusion quality measures are able to give us a very good notion of the algorithm fusion performance. According to Piella and Heijmans, if the value obtained by these indices is close to 1, then the composite final fused image will have higher quality characteristics, indicating the algorithm's performance level.

Table 1 shows the Q , Q_{Wt} , and Q_E results from applying these fusion quality measures to the product of proposed fusion algorithm, thus the Q_E result was obtained by applying the α value to 0.2, indicating the quantity of edge information from every image is contributing to fused image. Then having a higher Q_E index, we expect the final fused image will have a high visual quality. Finally, the saliency

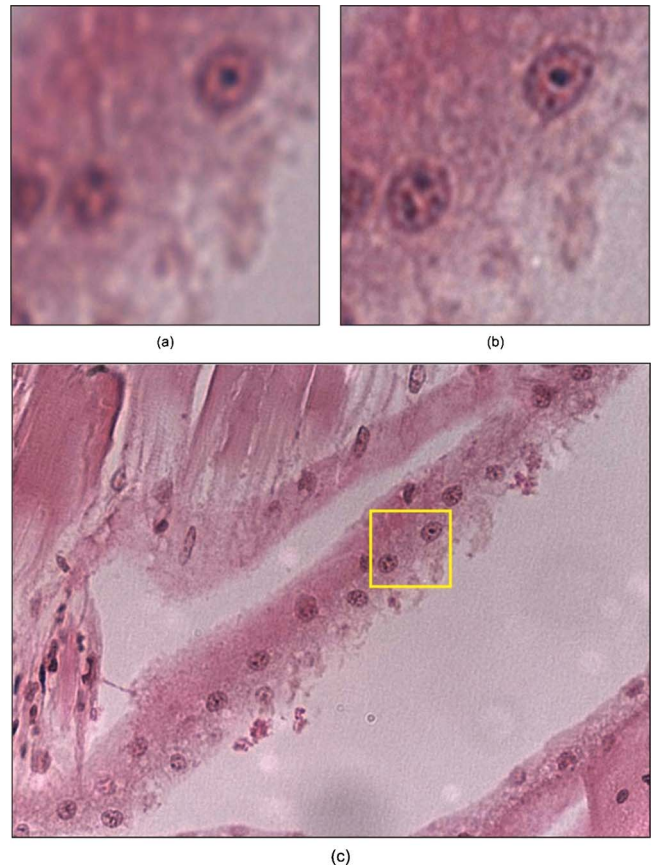


Fig. 3 Example of visual differences inside zoomed window shown in (c), between (a) the focused image and (b) the fused image from shrimp tissue sample.

used to compute the indices was the local variance applied to a window w_s with 351×351 pixels. This window size was selected because of the computer processing time. However, using smaller size windows to calculate the quality index does not significantly improve the quality results from the quality indices. To compute Q_E , the Laplacian gradient was used to extract the edge information of every image involved in the fusion process. Table 1 also shows the fusion algorithm quality measures from other fusion techniques, where the proposed algorithm is compared with the Laplacian gradient fusion technique, the ratio and averaging pyramid, and the DWT and the DCT fusion methods.

5 Conclusions

A new fusion method for color images was presented. This new algorithm offers significant performance when several images must be interpreted with high visual quality. Thus, the proposed algorithm will be suitable for implementation in real-time processing. This is due to the algorithm's robustness and accuracy in fusing several types of real images obtained from different kinds of samples. The algorithm was tested in different illumination conditions, bright and dark fields, and with several image resolutions capture.

Acknowledgments

Part of this work was supported by the Mexican National Council of Science and Technology (CONACYT, project

36075-B). Thanks to Dr. Ron Caro of Pepperdine University for his valuable comments and editing of this paper.

References

1. P. Hill, N. Canagarajah, and D. Bull, "Image fusion using complex wavelets," in *Proc. Br. Machine Vision Conf.* (2002).
2. Y. Zheng, E. A. Essock, and B. C. Hansen, "An advanced image fusion algorithm based on wavelet transform: Incorporation with PCA and morphological processing," in *Image Processing, Proc. SPIE 5298*, 177–187 (May 2004).
3. M. G. Forero, F. Sroubek, J. Flusser, R. Redondo, and G. Cristóbal, "Automatic screening and multifocus fusion methods for diatom identification," in *Applications and Science of Neural Networks, Fuzzy Systems and Evolutionary Computation VI, Proc. SPIE 5200*, 197–206 (Dec. 2003).
4. O. Rockinger, "Pixel level fusion of image sequences using wavelet frames," in *Proc. 16th Leeds Annual Statistical Research Workshop*, Leeds University Press, pp. 149–154 (1996).
5. I. Bloch and H. Maitre, "Data fusion in 2D and 3D image processing: An overview," in *Proc. Graphics and Image Processing, SIBGRAPI*, Campos do Jordao, Brazil, pp. 127–134 (1997).
6. I. Bloch and H. Maitre, "Image fusion," in *Proc. Int. Science Foundation Workshop on Data Mining*, Granada, Spain (1997).
7. R. K. Sharma and M. Pavel, "Adaptive and statistical image fusion," *Soc. Inf. Displ. Digest XXVII*, 969–972 (May 1996).
8. S. Li, J. T. Kwok, and Y. Wang, "Multifocus image fusion using artificial neural," *Pattern Recogn. Lett.* **23**(8), 985–997 (2002).
9. V. Petrovic, "Multilevel image fusion," *Proc. SPIE 5099*, 87–96 (Apr. 2003).
10. T. Achalakul, P. D. Haaland, and S. Taylor, "Math web: A concurrent image analysis tool suite for multispectral data fusion," *Proc. SPIE 3719*, 351–358 (Mar. 1999).
11. Z. Wang and A. C. Bovik, "A universal image quality index," *IEEE Signal Process. Lett.* **9**(3), 81–84 (2002).
12. G. Piella and H. Heijmans, "A new quality metric for image fusion," in *Proc. Int. Conf. on Image Processing, CWI*, Amsterdam, Netherlands, Vol. 3, pp. 173–176 (2003).
13. J. L. Pech-Pacheco, G. Cristóbal, I. Chamorro-Martínez, and J. Fernández-Valdivia, "Diatom autofocusing in lighting microscopy: A comparative study," in *Proc. Int. Conf. on Pattern Recognition*, Barcelona, Spain, pp. 318–321 (2000).
14. W. Bocker, W. Rolf, W. Muller, and C. Streffer, "Investigations about autofocus-algorithms for fluorescent-microscopy," *Applications of Digital Image Processing XIX, Proc. SPIE*, **2847**, 445–456 (1996).
15. M. Subbarao and A. Nikzad, "Focusing techniques," *Opt. Eng.*, **32**(11), 2824–2836 (1993).
16. T. Yeo, S. Ong, L. Jayasooriah, and R. Sinniah, "Autofocusing for tissue microscopy," *Image Vis. Comput.*, **11**(10), 629–639 (1993).
17. L. K. Firestone, K. Cook, K. Culp, N. Talsania, and K. Preston, "Comparisons of autofocus methods for automated microscopy," *Cytometry* **12**, 195–206 (1991).
18. E. Krotkov, "Focusing," *Int. J. Comput. Vis.* **1**, 223–237 (1987).
19. F. Groen, I. T. Young, and G. Ligthard, "A comparison of different focus functions for use in autofocus algorithms," *Cytometry* **6**, 81–91 (1985).
20. F. R. Boddeke, L. J. Van Vliet, H. Netten, and I. T. Young, "Autofocusing in microscopy based on the OTF and sampling," *Bioimaging* **2**, 193–203 (1994).
21. W. K. Pratt, *Digital Image Processing*, 2nd ed., pp. 62–72, Wiley Interscience Press, (1991).
22. V. Nikulin and G. Bebis, "Multiresolution image retrieval through fusion," in *Storage and Retrieval Methods and Applications for Multimedia, Proc. SPIE 5307*, 377–387 (Jan. 2004).
23. "Studio encoding parameters of digital television for standard 4:3 and widescreen 16:9 aspect ratios," ITU-R BT.601-5 (1995).
24. V. G. Devereux, "Limiting of YUV digital video signals," BBC Research Department Report BC RD1987 22 (1987).
25. V. Kober, M. Mozerov, J. Alvarez-Borrego, and I. A. Ovseyevich, "An efficient algorithm for suppression of impulse noise in color images," *Pattern Recogn. Image Anal.*, **15**(1), 219–222 (2005).
26. G. Piella, "New quality measures for image fusion," in *Proc. 7th. Int. Conf. of Information Fusion*, pp. 542–546, Stockholm (Jun. 2004).
27. V. Petrovic and X. Costas, "Evaluation of image fusion performance with visible differences," in *Proc. ECCV, LNCS 3023*, pp. 380–391, Springer, (2004).
28. M. A. Bueno, J. Álvarez-Borrego, L. Acho, and M. C. Chávez-Sánchez, "Fast autofocus algorithm for automated microscopes," *Opt. Eng.* **44**(6), 063601 (2004).



Mario A. Bueno received his MEng degree in automation and control at Universidad Autónoma de Ciudad Juárez (UACJ) in 1996, and his PhD in communication and electronics at CITEDI-IPN in 2005. His work is related on biological image processing topics.



Josué Alvarez-Borrego received his BS degree in physical oceanography in 1981 from the Facultad de Ciencias Marinas, Ensenada, B.C., Mexico and his MSc and PhD degrees in Optics in 1983 and 1993 from CICESE, Mexico. He is a titular researcher with the Dirección de Telemática, CICESE, Mexico. His research interests are image processing with applications to biogenic particles and image processing of the sea surface. Author of several scientific papers and scientific conferences. He is a member of the Mexican Academy of Optics, Researches National System (SNI), and the Sciences Mexican Academy.



Leonardo Acho received his MSc degree in electronics systems at ITESM-Monterrey, Mexico in 1992 and his PhD degree in automatic control from CICESE, Mexico in 2001. Now, he is with the Digital Technology Research and Development Center (CIT-EDIIPN), Mexico.



María Cristina Chávez-Sánchez received her biological degree in 1971, her MSC in 1983 and her PhD in aquaculture and fisheries management in 1987 from the Stirling University. Currently she is researcher in the Mazatlan Unit on Aquaculture and Environmental Management of the Research Center of Feeding and Development (CIAD, A.C.). Her research interest is aquatic pathology.